

MITIGATING DYNAMIC STALL WITH A MOVABLE LEADING-EDGE: THE NACA0012-IK30 WING

Emanuel A. R. Camacho^{1,2}, André R. R. Silva¹ & Flávio D. Margues²

¹AEROG-LAETA, University of Beira Interior (UBI), 6201-001 Covilhã, Portugal ²LABDIN-EESC, University of São Paulo (USP), 13566-590, São Paulo, Brazil

Abstract

One major problem that affects rotor blade aerodynamics is dynamic stall, characterized by a series of events where transient vortex shedding negatively affects drag and lift, leading to abrupt changes in the wing's pitching moment. The present work focuses on the mitigation of such effects by using a modified NACA0012 airfoil: the NACA0012-IK30 airfoil, used previously for thrust enhancement in flapping propulsion. An experimental rig is designed and built to study the advantages of a time-varying pitching leading edge on a plunging wing, more specifically its influence on the aerodynamic coefficients over time. Results indicate that when the wing is not experiencing significant stall, the movable leading edge does not hold considerable influence on drag or lift. However, it can reduce the pitching moment intensity by indirectly shifting the pressure center. Contrarily, when the wing is under proper dynamic stall, the movable leading edge truly improves the aerodynamic characteristics while operating at smaller effective angles of attack. This study contributes to the long-standing discussion on how to mitigate the adverse effects of dynamic stall by providing an innovative yet simple solution.

Keywords: Dynamic stall; Force measurements; Movable leading-edge; Flow control

1. Introduction

Dynamic stall is a central topic in unsteady aerodynamics, mainly because it is a synonym for performance degradation in helicopter rotor blades. It is characterized as a vorticity eruption from the airfoil where typically a leading-edge vortex (LEV) is formed and is later convected on the surface, producing undesirable oscillations in aerodynamic loads [1]. These effects can quickly couple with structural dynamics and contribute to accelerated fatigue, which when not considered seriously can lead to structural failure [2]. Dynamic stall is also part of natural flight and swimming, also playing an important role when it comes to the design of innovative energy harvesters that use flapping foils [3]. Oscillating structures subjected to the dynamic stall regime are highly dependent on several geometric and kinematic parameters such as the angle of attack and pitch rate. For instance, Francis and Keesee [4] saw that when the airfoil undergoes rapid and large-amplitude pitching motions at a constant rate, the airfoil can offer close to three times the lift compared to quasi-steady values. This is justified by the presence of a high energy separation vortex located at the leading edge which dominates force generation as it convects downstream, as corroborated by Favier et al. [5] who studied a combined translation/pitch motion of a NACA0012 airfoil.

This leading-edge vortex was also noticed by Lorber and Carta [6] as a central mechanism of the unsteady aerodynamic response during and after stall. They looked at the aircraft poststall maneuvers and helicopter high-speed forward flight regimes and concluded that this vortex strengthens with a higher pitch rate and loses its intensity with the Mach number and the proximity to the steady-state stall angle. However, as noted by Visbal [7], at the upper range of Mach number, the dynamic stall process is more influenced by the boundary layer and shock interaction rather than by the formation of a leading-edge vortex. The dynamics of this vortex have been studied both experimentally and numerically by Wernert et al. [8] when testing a pitching airfoil. They present four distinct phases that

generally characterize the dynamic stall phenomena: attached flow, leading-edge vortex formation followed by poststall vortex shedding, and finally, reattachment. The onset phase was analyzed by Geissler and Haselmeyer [9] who looked at specific dynamic stall triggers, for instance, transitional flow influence, comprehensibility effects, and the presence of boundary-layer tripping devices. Understanding these fundamental concepts is crucial to avoid or mitigate the adverse effects of dynamic stall.

But dynamic stall should not be looked at as something exclusively detrimental. Looking beyond common aeronautical applications, the dynamic stall is a key part of natural flight, where it is a byproduct of thrust generation. Isogai et al. [10] looked into this topic by studying the effects of dynamic stall on the propulsive characteristics of a flapping airfoil, concluding that a less intense LEV formation is required for good propulsive efficiency. But when it comes to thrust generation, the leading-edge vortex acts as a boosting mechanism, as verified fairly recently by Camacho et al. [11] when conducting the propulsive optimization of the IK30 mechanism at the lower Reynolds number range. Moreover, at these smaller length scales, there are gigantic differences in how animals fly. Birds and insects present distinctive ways of flying, with the first preferring slower oscillating cycles while the latter flap their wings energetically, creating strong whirls and eddies that surround them and act as lift boosters [12]. Hence, the dynamic stall occurrence must be analyzed carefully based on the regime and environment to conclude if its effects are truly negative.

Nevertheless, when it comes to higher Reynolds environments, the presence of a LEV typically degrades the aerodynamic performance. Hence, there is a general interest in mitigating the adverse effects, either using active or passive devices. Visbal and Garmann [13] used a very-high frequency and low-amplitude zero-net mass flow blowing/suction slot located on the wing lower surface close to the leading edge and observed that these oscillations have the potential to inhibit the leading-edge separation bubble and thus, the formation of large dynamic stall vortices. The same concept was then used to control the dynamic stall but in a finite swept wing [14]. Another technique used by Niu et al. [15] is a variable droop leading edge where one can locally change the angle of attack near the leading edge. Results indicate that drag is reduced, lift is kept at a higher level and the nose-down tendency after stall is very much reduced. Morphing technologies are also an adequate solution to mitigate stall occurrence, showing the capability of delaying the stall angle coupled with an increase in lift production [16]. Additionally, the natural world can also provide good solutions when trying the reduce the adverse effects of dynamic stall, as shown by Liu et al. [17], who saw that wingtip slots reduce the adverse pressure gradient, improving the wing's performance. Moreover, when further modifying the wing, for instance, adding dihedral, the wing can have its gliding capabilities improved considerably.

The present paper has the same motivation of mitigating the effects of the dynamic stall by using a modified version of the commonly used NACA0012 airfoil: The NACA0012-IK30 airfoil. It was first introduced to improve the propulsive capabilities of a flapping airfoil, and demonstrated to be useful in increasing both thrust and propulsive efficiency [18]. With its movable leading edge, the airfoil is now used with a different purpose: the mitigation of dynamic stall under plunging oscillations. The methodology section provides information regarding the leading-edge activation, followed by the results where the efficacy of the mechanism is discussed.

2. Methodology

The NACA0012-IK30 airfoil was tested experimentally at the Laboratory of Dynamics (EESC-USP) by conducting force measurements in a wind tunnel. The wind tunnel is a subsonic blower capable of providing a volumetric flow rate of $400\,\mathrm{m^3\,min^{-1}}$, which at the outlet section represents approximately $27\,\mathrm{m\,s^{-1}}$. The wind speed is controlled by measuring the equivalent airspeed using a VECTUS TIVA manometer, which is then corrected to obtain the true airspeed. The temperature and pressure are measured using the MT-241A thermo-hygrometer and the VECpress 201 micromanometer, respectively. The temperature is also used to calculate the dynamic viscosity, using Sutherland's law.

The wing under testing is placed right at the outlet section of the wind tunnel without any walls surrounding it to avoid any blockage effects. Its wet area has an aspect ratio of 2.5, a chord of $20\,\mathrm{cm}$, and a wingspan of $0.6\,\mathrm{m}$. It is designed with the aforementioned NACA0012-IK30 airfoil that is

simply a sliced version of the conventional NACA0012, as illustrated in Figure 1. Detailed geometric information can be seen in [18].

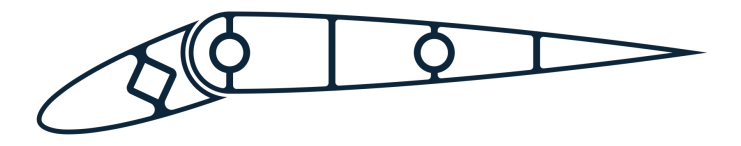


Figure 1 – The NACA0012-IK30 airfoil.

Concerning wing motion control, three motors are used to accomplish the desired kinematics: a stepper motor for pitch adjustments (KTC-KML093-F07), another for the plunging motion (KTC-HT23-402.8 with a gear reduction of 1:4 connected to a linear guide) and a servo motor (SRT DL3017) for the leading-edge actuation. As observed in Figure 2, the servo motor is placed at the wing tip in a special hub, linked to a rotational mechanism that allows the leading edge to rotate at the wing's maximum thickness position, 0.3c. The first two motors are connected to STR8 drivers that offer a resolution ranging from 200 PPR (Pulses per Revolution) up to 20000 PPR.

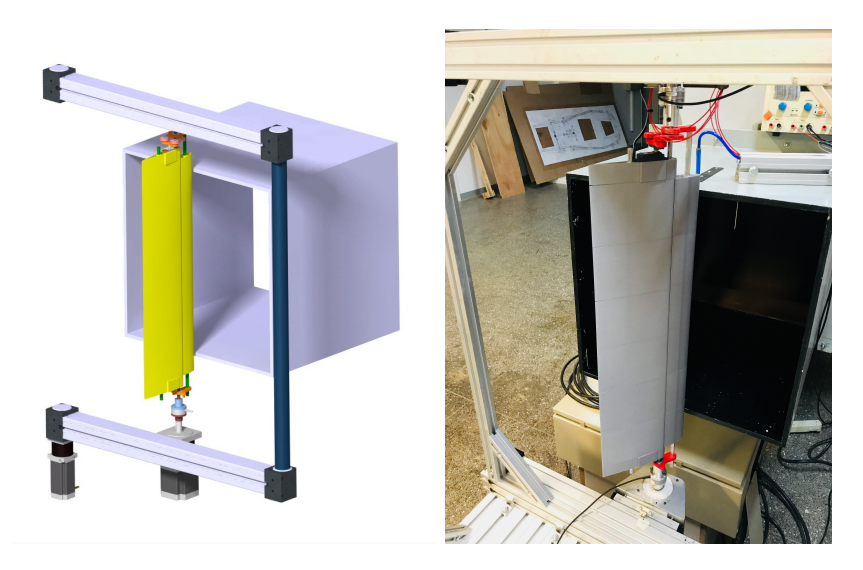


Figure 2 – Experimental setup for force measurements.

The prescribed kinematics are accomplished by implementing a Simulink model, which runs simultaneously in a dSpace board (DS2101) and an Arduino Uno microcontroller board, at $10\,\mathrm{kHz}$ and $1\,\mathrm{kHz}$, respectively. The dSpace board is connected directly to the stepper's drivers which transmit steps and direction information through PWM signals, while the servo motor receives instructions from the Arduino board using the already available Arduino MATLAB/Simulink packages.

Regarding force measurements, two ATI mini40 force and torque sensors were placed at the wing extremities. These were connected to a dSpace DS2004 board, which runs the same Simulink model used for kinematics. In Figure 3, relevant parameters used to analyze the wing are shown, as is the sensor positioning. The sensors have their z-axis aligned with the pivot axis of the airfoil and since the stepper used for pitching only controls the back part (ψ part) angle of attack, forces are measured at the ψ -part body axis. All forces and moments are affected by an uncertainty of $0.5\,\mathrm{N}$ and $0.03\,\mathrm{N}\,\mathrm{m}$, respectively. All measured data is filtered with a 8^{th} -order Butterworth filter with a cutoff frequency of $5\,\mathrm{Hz}$.

Concerning the prescribed kinematics, the present paper is focused exclusively on the plunging motion coupled with a pitching leading edge. Sinusoidal waves are selected for both motion components, with plunging given by

$$y = A\sin(2\pi ft),\tag{1}$$

where A and f are the motion amplitude and frequency, respectively. The leading edge angle of

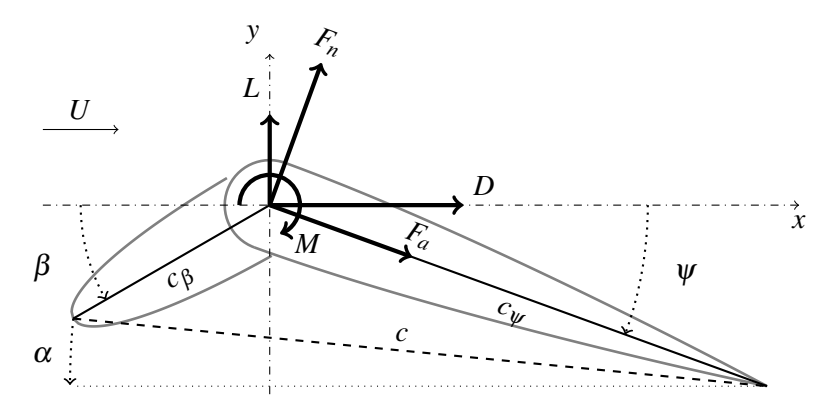


Figure 3 – NACA0012-IK30 airfoil nomenclature.

attack is prescribed as

$$\beta = \overline{\beta} + A_{\beta} \sin(2\pi f t + \phi) \text{ (with } \overline{\beta} = \psi - A_{\beta}), \tag{2}$$

where A_{β} is the pitching amplitude and ϕ is the phase angle between the wing's plunging and the leading-edge activation, which throughout the study is fixed at 90° . $\overline{\beta}$ is chosen so the leading-edge does not surpass the fixed ψ angle. For a quick visualization of the desired kinematics, Figure 4 shows the oscillating cycle, assumed to start half-way down.

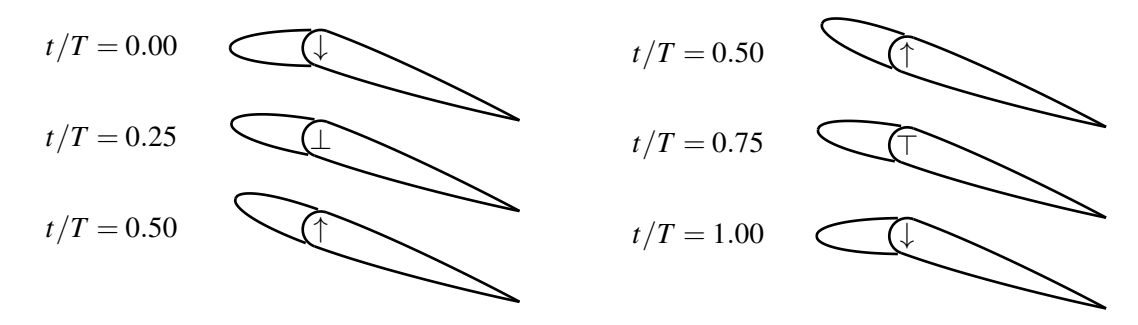


Figure 4 – Plunging kinematics.

3. Results

Before moving to the discussion of the aerodynamic coefficients, we start by presenting the conditions that the wing was subjected to. The wing is tested at a Reynolds number of 2.0×10^5 with a nondimensional amplitude of 0.5, three nondimensional velocities (0.0125, 0.0250, 0.0375) and three ψ values, 10° , 15° and 20° . For each one of these conditions, β is changed dynamically with different pitching amplitudes. These conditions are shown in Figure 5 which illustrates the kh domain, together with the motor limitation due to software ($\approx 0.7 \, \mathrm{m \, s^{-1}}$).

The first set of results, shown In Figure 6, considers the three reduced frequencies (obtained from the imposed nondimensional velocities) illustrated in the study domain, with ψ fixed at 10° . For each one of these conditions, two leading-edge pitching amplitudes, 0° and 5° are tested. All three aerodynamic coefficients are plotted both against time (t/T) and the effective angle of attack. The latter is defined as

$$\alpha_{\text{eff}} = \arctan\left(-\frac{\dot{y}}{U}\right) + \arctan\left(\frac{c_{\beta}\sin\beta + c_{\psi}\sin\psi}{c_{\beta}\cos\beta + c_{\psi}\cos\psi}\right) \tag{3}$$

which can be mathematically deduced from Figure 3. Before advancing to the analysis of the aerodynamic performance, it is important to mention that results do not hold up a two-dimensional assumption, meaning that three-dimensional effects on dynamic stall cannot be neglected. Nevertheless, the main focus here is observing if the proposed wing is indeed capable of mitigating the adverse effects. Still, 3D dynamic stall characteristics of aerodynamic surfaces are an important area of study.

On the first and fourth rows (Figure 6), the drag coefficient is shown over the plunging cycle. Results show that activating the leading edge, which results in a reduction in the effective angle of attack

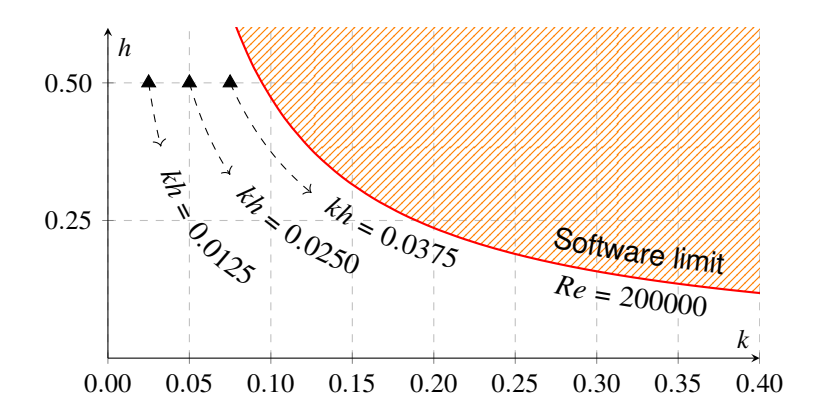


Figure 5 – Tested conditions in the *kh* domain. Values are calculated based on a representative pressure of 915 hPa and a temperature of 25.0 °C.

has a slight effect on the drag coefficient, though not considerable. The reduction comes primarily from the lowering of pressure drag and not because of mitigating flow separation. No massive flow separation is expected as the maximum effective angle of attack experienced during the oscillation does not come near the static stall angle (around 15°), verified during preliminary steady cases. Lift (second and fifth rows) also stays fairly constant regardless of A_{β} , meaning that the same lift coefficient can be obtained at a lower effective angle of attack. This means that at this ψ of 10° , a condition where the wing does not experience dynamic stall, deflecting the leading edge for drag reduction and lift enhancement is rather useless. Moreover, the allowable reduced frequency range selected throughout the study did not hold any considerable influence apart from a slight increase in the magnitude of coefficients.

However, when it comes to the moment coefficient (third and sixth rows), we see a considerable reduction in its mean value by activating the leading edge. Since drag and lift stay nearly the same, the lowering of the pitching moment can only be caused by the shift of the pressure center. The change in the pressure center location is highly affected by the place of the suction peak zone: when the leading edge has no pitching, the suction zone stays mostly at the front of the wing, while when the leading edge drops down, this low-pressure zone moves downstream closer to the pivot point, thus reducing the moment measured. This is a clear advantage of the proposed wing, where torsional effects on the wing are reduced.

Increasing the ψ to 15° , shown in Figure 7, produces different aerodynamic effects. Starting with the drag coefficient when no leading-edge deflection is present ($A_{\beta}=0^{\circ}$), we see that it is now more dependent on the motion phase, reaching its peak value during descent. This is justified by the appearance of separated flow due to surpassing the static stall angle, somewhere close to 15° . As expected, the peak value increases with k as it contributes to a higher effective angle of attack. With a pitching leading edge ($A_{\beta}=7.5^{\circ}$), the overall drag becomes smaller, proving that lowering the effective angle of attack by modifying β is an effective way to control the flow around the plunging airfoil.

Improvements are also seen in the lift coefficient, although not as visible as in drag. Nevertheless, the wing clearly shows that it can benefit from a movable leading edge. The moment coefficient, unlike the previous condition, does not change in terms of peak magnitude, though there is a difference in the waveform, especially during the descending phase, where dynamically activating the β part reduces the nose-up tendency of the wing.

In Figure 8, the condition where $\psi=20^\circ$ is shown. For this specific case three leading-edge pitching amplitudes are used: $A_\beta=0^\circ,~5^\circ,$ and $10^\circ.$ At this angle, the wing is well beyond its static stall angle, meaning that it is experiencing proper dynamic stall. As seen ahead, in the presence of a considerable stall, the movable leading edge presents an enormous impact on the aerodynamic performance.

Looking at the drag coefficient, we see that regardless of reduced frequency, the plunging-only condition produces a substantial amount of drag. With a leading-edge pitching amplitude of just $A_{\beta} = 5^{\circ}$, a drag reduction is visible, going down even further when $A_{\beta} = 10^{\circ}$. Lift is affected the other way

around, with the pitching leading edge increasing lift production. This indicates that the stall phenomenon is being relieved, particularly during the descending phase, when the leading edge droops down, indicating flow reattachment.

This is corroborated by the moment coefficient graphs, which, unlike previous conditions, there is an increase in the nose-up tendency of the wing with the activation of the leading edge. This is the typical response when a flow reattachment happens since it revives a stronger suction peak zone close to the leading edge which itself moves the pressure center upstream, intensifying the nose-up tendency. Although being a disadvantage due to higher torsional loads, the gains in lift and improvement of drag may justify it.

4. Conclusion

The present work focused on the topic of mitigating the adverse effects of dynamic stall by proposing an innovative geometrical modification to the commonly used NACA0012 airfoil. The airfoil was built into a wing which is mounted in an experimental rig designed to measure the forces of oscillating airfoils. After validation and calibration of the experimental setup, tests were conducted at a Reynolds number of 2×10^5 , for a nondimensional amplitude of 0.5 and three different nondimensional velocities. For the range studied, the plunging velocity did not have a considerable effect on the aerodynamic phenomena, with the only visible difference being the coefficients magnitude. The crucial variable of the study was indeed the leading-edge pitching amplitude, coupled with the mean angle of attack. These have a direct impact on the frontal area angle of attack, which as observed, can reduce drag, provide a noticeable lift improvement, and in some conditions, reduce the pitching moment. Nevertheless, the leading-edge device must be used wisely to avoid degrading the wing's performance even further from the dynamic stall regime.

The study demonstrated the efficacy of dynamically moving the frontal area of the airfoil, which that can be implemented in so many areas. Similar studies must be made to find innovative and optimal solutions that can provide an additional boost in rotor performance but also in different topics such as bio-inspired vehicles that use flapping wings as their means of propulsion.

5. Funding

The present work was performed under the scope of the Aeronautics and Astronautics Research Center (AEROG) of the Laboratório Associado em Energia, Transportes e Aeronáutica (LAETA) activities, and it was supported by Fundação para a Ciência e Tecnologia (FCT) through the project numbers UIDB/50022/2020, UIDP/50022/2020, LA/P/0079/2020 and the grant sponsored by Fundação para a Ciência e Tecnologia 2020.04648.BD. F. D. Marques acknowledges the financial support of the Brazilian National Council for Scientific and Technological Development (CNPq grants #306698/2023-4).

6. Contact Author Email Address

Contact us using earc.aerog@gmail.com or +351 910051301.

7. Copyright Statement

The authors confirm that they, and/or their company or organization, hold copyright on all of the original material included in this paper. The authors also confirm that they have obtained permission, from the copyright holder of any third party material included in this paper, to publish it as part of their paper. The authors confirm that they give permission, or have obtained permission from the copyright holder of this paper, for the publication and distribution of this paper as part of the ICAS proceedings or as individual off-prints from the proceedings.

References

- [1] Norman D. Ham. Aerodynamic loading on a two-dimensional airfoil during dynamic stall. *AIAA Journal*, 6(10):1927–1934, October 1968. [Crossref].
- [2] Thomas C. Corke and Flint O. Thomas. Dynamic stall in pitching airfoils: Aerodynamic damping and compressibility effects. *Annual Review of Fluid Mechanics*, 47(1):479–505, January 2015. [Crossref].
- [3] Bo Wang, Bing Zhu, and Wei Zhang. New type of motion trajectory for increasing the power extraction efficiency of flapping wing devices. *Energy*, 189:116072, dec 2019. [Crossref].

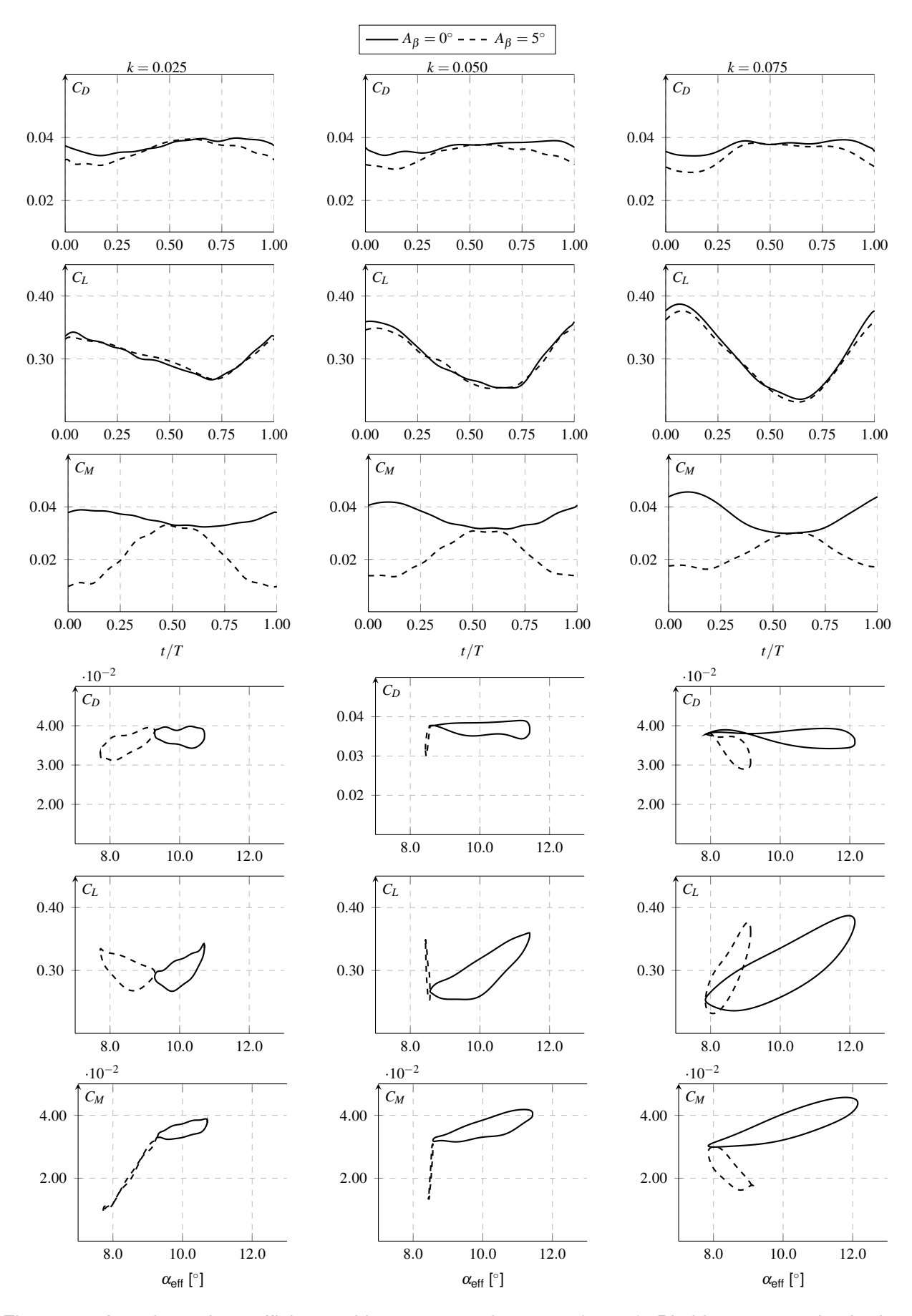


Figure 6 – Aerodynamic coefficients with h=0.50 and $\overline{\psi}=10^\circ$ ($\dot{\psi}=0$). Pitching moment is obtained at the pivot point (0.3c).

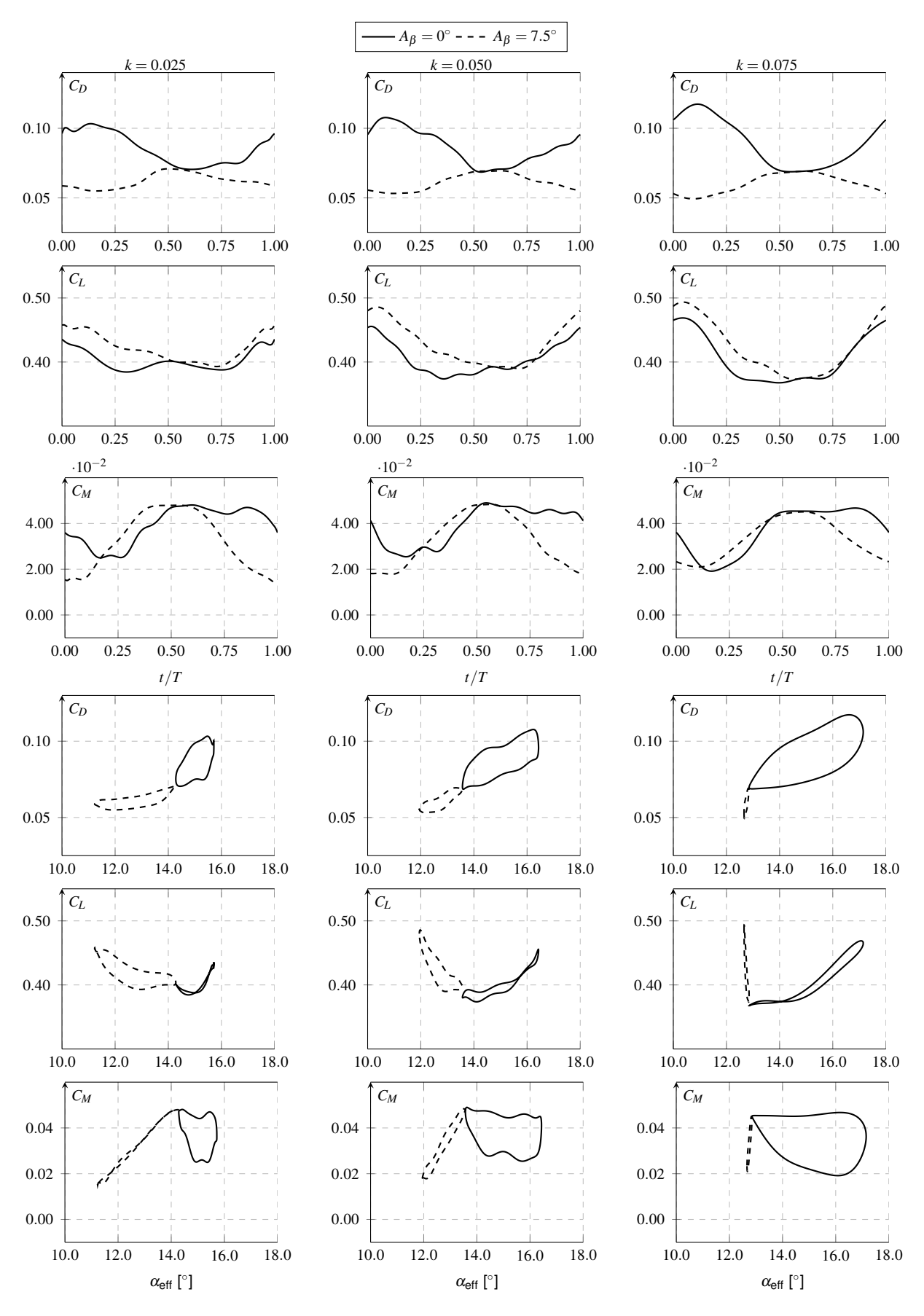


Figure 7 – Aerodynamic coefficients with h=0.50 and $\overline{\psi}=15^{\circ}$ ($\dot{\psi}=0$). Pitching moment is obtained at the pivot point (0.3c).

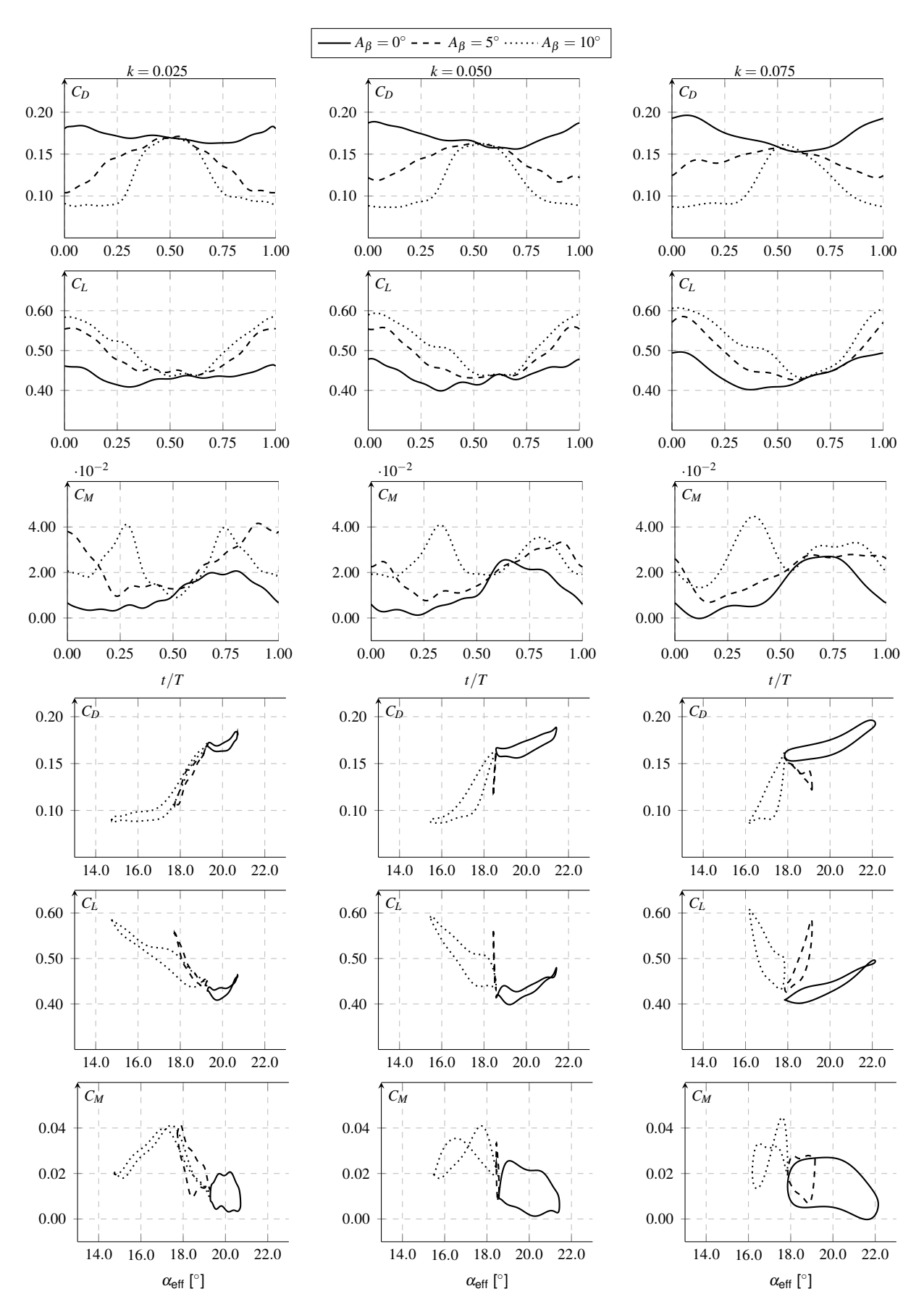


Figure 8 – Aerodynamic coefficients with h=0.50 and $\overline{\psi}=20^{\circ}$ ($\dot{\psi}=0$). Pitching moment is obtained at the pivot point (0.3c).

- [4] M. S. Francis and J. E. Keesee. Airfoil dynamic stall performance with large-amplitude motions. *AIAA Journal*, 23(11):1653–1659, nov 1985. [Crossref].
- [5] D. Favier, A. Agnes, C. Barbi, and C. Maresca. Combined translation/pitch motion a new airfoil dynamic stall simulation. *Journal of Aircraft*, 25(9):805–814, sep 1988. [Crossref].
- [6] Peter F. Lorber and Franklin O. Carta. Airfoil dynamic stall at constant pitch rate and high reynolds number. *Journal of Aircraft*, 25(6):548–556, jun 1988. [Crossref].
- [7] Miguel R. Visbal. Dynamic stall of a constant-rate pitching airfoil. *Journal of Aircraft*, 27(5):400–407, may 1990. [Crossref].
- [8] Philippe Wernert, Wolfgang Geissler, Markus Raffel, and Juergen Kompenhans. Experimental and numerical investigations of dynamic stall on a pitching airfoil. *AIAA Journal*, 34(5):982–989, may 1996. [Crossref].
- [9] W. Geissler and H. Haselmeyer. Investigation of dynamic stall onset. *Aerospace Science and Technology*, 10(7):590–600, oct 2006. [Crossref].
- [10] K. Isogai, Y. Shinmoto, and Y. Watanabe. Effects of Dynamic Stall on Propulsive Efficiency and Thrust of Flapping Airfoil. *AIAA Journal*, 37(10):1145–1151, oct 1999. [Crossref].
- [11] Emanuel A.R. Camacho, André R.R. Silva, and Flávio D. Marques. Optimal leading-edge deflection for flapping airfoil propulsion. *Proceedings of the Institution of Mechanical Engineers, Part G: Journal of Aerospace Engineering*, 237(16):3640–3653, September 2023. [Crossref].
- [12] Neil Savage. Aerodynamics: Vortices and robobees. Nature, 521(7552):S64-S65, May 2015. [Crossref].
- [13] Miguel R. Visbal and Daniel J. Garmann. Mitigation of dynamic stall over a pitching finite wing using high-frequency actuation. *AIAA Journal*, 58(1):6–15, January 2020. [Crossref].
- [14] Daniel J. Garmann and Miguel R. Visbal. Control of dynamic stall on swept finite wings. *AIAA Journal*, 60(9):5262–5272, September 2022. [Crossref].
- [15] Jianping Niu, Juanmian Lei, and Tianyu Lu. Numerical research on the effect of variable droop leading-edge on oscillating NACA 0012 airfoil dynamic stall. *Aerospace Science and Technology*, 72:476–485, jan 2018. [Crossref].
- [16] Sijia Jia, Zhenkai Zhang, Haibo Zhang, Chen Song, and Chao Yang. Wind tunnel tests of 3d-printed variable camber morphing wing. *Aerospace*, 9(11):699, November 2022. [Crossref].
- [17] Dan Liu, Wenqing Yang, and Bifeng Song. Numerical simulation on aerodynamic performance of bird-like flapping wing with slotted-tip. 2021.
- [18] Emanuel A. R. Camacho, Flávio D. Marques, and André R. R. Silva. Influence of a deflectable leading-edge on a flapping airfoil. *Aerospace*, 10(7):615, July 2023. [Crossref].